Journal of Geoscience and Environment Protection, 2025, 13(1), 156-177
https://www.scirp.org/journal/gep
ISSN Online: 2327-4344
ISSN Print: 2327-4336

Analysis of Spatiotemporal Trends and Variability in Precipitation Extremes over Tanzania during 1981-2023

Ombeni Habibu Msuya[1,2], Zhao Yu[1], Stephano Daniel Semgomba[1,2]

[1]Key Laboratory of Meteorological Disaster of Ministry of Education (KLME), International Joint Research Laboratory of Climate and Environment Change (ILCEC), Collaborative Innovation Center on Forecast and Evaluation of Meteorological Disasters (CIC-FEMD), School of Atmospheric Sciences, Nanjing University of Information Science & Technology, Nanjing, China
[2]Forecasting Department, Tanzania Meteorological Authority (TMA), Dodoma, Tanzania
Email: ombenimsuya@rocketmail.com, zy0817@126.com

How to cite this paper: Msuya, O. H., Yu, Z., & Semgomba, S. D. (2025). Analysis of Spatiotemporal Trends and Variability in Precipitation Extremes over Tanzania during 1981-2023. *Journal of Geoscience and Environment Protection, 13,* 156-177.
https://doi.org/10.4236/gep.2025.131009

Received: December 16, 2024
Accepted: January 17, 2025
Published: January 20, 2025

Abstract

This study examines the spatiotemporal trends and variability of precipitation extremes across Tanzania from 1981 to 2023, focusing on role of oceanic systems and large-scale climate phenomena. The analysis employed standardized extreme precipitation indices recommended by the Expert Team on Climate Change Detection and Indices. Spatial and temporal patterns were evaluated using empirical orthogonal function analysis, while Pearson correlation coefficients and the Mann-Kendall test were used to determ8ine the significance of trends and relationships. The results highlight pronounced spatial contrasts, with central and southern regions experiencing more intense and frequent extreme rainfall, including consecutive wet days, heavy precipitation events, and higher daily rainfall intensities. These regions exhibit significant upward trends, indicating heightened vulnerability to extreme wet conditions, while the northern areas experience fewer wet spells and lower overall precipitation. The first principal component captures a pattern of intensified precipitation in the southern and central regions, whereas the second principal component reveals a north-south gradient characterized by sustained moderate rainfall in the north and intense, short-duration rainfall in the south. Large-scale climate oscillations, including the Atlantic Multidecadal Oscillation, the El Niño-Southern Oscillation, the Indian Ocean Dipole, and the Pacific Decadal Oscillation, play a critical role in shaping regional precipitation extremes. These phenomena influence the frequency, spatial distribution, and intensity of rainfall through mechanisms such as atmospheric pressure anomalies, moisture convergence, and cyclonic activity. For instance, high-pressure systems in the North Pacific suppress rainfall, while cyclonic systems in the eastern Indian Ocean enhance convective activity and moisture availability.

Keywords

Extreme Precipitation, Precipitation Indices, Oceanic Systems, Tanzania

1. Introduction

Climate change has dramatically altered precipitation patterns across the globe, with wide-ranging implications for natural ecosystems, human societies, and the global water cycle (Trenberth, 2011). Since the 1950s, the rapid increase in greenhouse gas concentrations has accelerated global warming, resulting in rising sea levels and the retreat of snow and ice covers (Brohan et al., 2006). This warming has significantly influenced the trends, frequency, and intensity of climate extremes, including unprecedented temperature and precipitation events, which are distributed unevenly across time and space (Alexander et al., 2006; Fan et al., 2014; Fischer & Knutti, 2015). Precipitation, as a key component of the hydrological cycle, plays a central role in regulating hydrometeorological processes. Variability in precipitation and associated extremes directly impacts natural ecosystems and human societies (Rosenzweig et al., 2002). Higher global temperatures and increased evaporation have resulted in heightened atmospheric water vapor, leading to more frequent storms, intensified rainfall events, and extended dry spells that contribute to land surface drying (Sharma et al., 2021). The impacts of extreme precipitation events, such as floods, droughts, and soil erosion, often exceed those of average climate conditions, significantly disrupting agricultural systems, water resources, and socio-economic development (Barrett & Santos, 2014; Lavell et al., 2012). Studies of extreme weather events, including heavy rainfall and prolonged droughts, have spanned different regions worldwide. Research in Canada (Li et al., 2018), India (Gautam & Bana, 2014), the United Kingdom (Otto, 2024), the United States (Mallakpour & Villarini, 2015), South Africa (Nangombe et al., 2018) and the Czech Republic (Elleder, 2015) has highlighted region-specific vulnerabilities to extreme weather. Increasingly, global assessments confirm that precipitation extremes, particularly in the Northern Hemisphere mid-latitudes, have become more frequent and intense (Alexander, 2016). In tropical regions, such as Singapore, the frequency and intensity of extreme precipitation have significantly risen over recent decades (Li et al., 2018).

Recently, East African countries have faced frequent floods that have displaced numerous communities and resulted in loss of life, these events underscore the critical necessity for robust disaster management and climate adaptation strategies in the region (Mafuru & Guirong, 2018). Tanzania, located between the East African Great Lakes and the Indian Ocean, faces unique challenges due to its geographic position. In recent years, Tanzania has experienced an increasing frequency of extreme events, including severe floods and prolonged droughts, which have severely impacted agriculture, human settlements, and ecosystems. Notable events such as the floods of 1997 and the drought of 2006 have underscored the

vulnerability of critical socio-economic sectors like agriculture (Kijazi & Reason, 2009). While previous studies have examined regional climate variability and its impacts, the extent to which large-scale climate drivers influence the frequency, intensity, and spatial distribution of extreme precipitation events in Tanzania remains poorly understood. Understanding its variability and intensity in space and time is essential for attributing changes to climate variability and long-term climate change (O'Gorman, 2015; Shiu et al., 2012). This study aims to investigate the linkages between large-scale atmosphere-ocean systems and extreme precipitation events in Tanzania. By analyzing trends and spatial patterns of precipitation extremes, this research seeks to enhance understanding of how global climate drivers affect local weather patterns. Such insights are critical for informing disaster management strategies, fostering ecosystem resilience, and guiding sustainable socio-economic development in the face of climate change.

The article is organized as follows: Section 2 provides an overview of the data sources and methodologies employed in this study. Section 3 examines the spatial and temporal characteristics of precipitation extremes across the study region. Section 4 explores the relationships between these precipitation extremes and key oceanic drivers, including the Atlantic Multidecadal Oscillation (AMO), Pacific Decadal Oscillation (PDO), El Niño-Southern Oscillation (ENSO), and Indian Ocean Dipole (IOD). Finally, Section 5 presents the conclusions, highlighting key findings and their implications for climate adaptation and management.

2. Data and Methodology

2.1. Study Area

Tanzania, situated in Eastern Africa just south of the equator, spans latitudes 1˚ to 12˚S and longitudes 29˚ to 41˚E. The country is composed of 883,749 km^2 of land and 59,050 km^2 of inland water bodies and sections of the Indian Ocean. Its diverse landscapes range from coastal plains with sandy beaches to expansive plateaus and towering mountains, offering an intricate tapestry of topographical and climatic features. The eastern coastline of Tanzania is a narrow strip of low-lying plains along the Indian Ocean, defined by a hot and humid tropical climate with year-round temperatures averaging 25˚C to 30˚C (Chang'a et al., 2017). Moving inland, the central plateau rises to elevations between 900 and 1,800 meters (3,000 to 5,900 feet), where the climate becomes milder, with temperatures ranging from 20˚C to 25˚C. To the west, the Great Rift Valley carves through the landscape, forming escarpments and valleys that experience a variety of climates, including cooler conditions in the highlands. Rainfall variability in Tanzania, driven by the Intertropical Convergence Zone (ITCZ), presents bimodal and unimodal patterns across different regions. Northern Tanzania experiences a bimodal pattern, with rainy seasons from March to May and October to December, while the southern and central regions exhibit a unimodal regime spanning November to April (Borhara et al., 2020; Nicholson, 2018) which is the study season of interest (**Figure 1**). The ITCZ's strength and position are influenced by trade wind systems,

which in turn are modulated by subtropical high-pressure systems and global climate phenomena such as the Indian Ocean Dipole and El Niño-Southern Oscillation (Ame et al., 2021; Nicholson, 2015). From the coastal tropics to the highland plateaus and mountainous regions, the country showcases how varied environments respond to regional and global climatic forces. The Indian Ocean plays a critical role, driving phenomena such as the Indian Ocean Dipole, El Niño, and La Niña, which strongly influence rainfall and temperature patterns. This remarkable variety not only underscores the complexity of Tanzania's climate but also highlights its importance in understanding broader climate variability. By examining the intricate interplay of these climatic zones, researchers can better unravel the impacts of climate change on ecosystems, human livelihoods, and natural resources in the region.

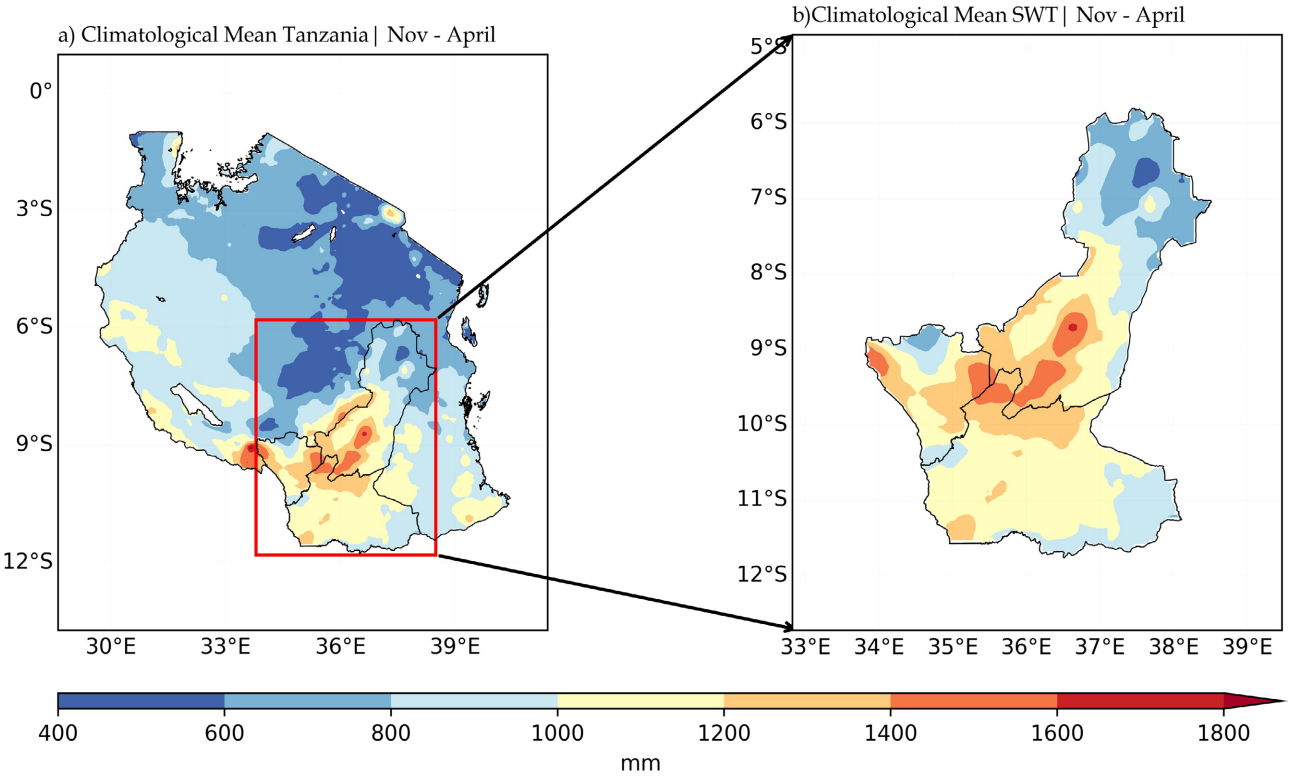

Figure 1. Study area; (a) Country climatology for Nov - Apr season during 1981-2023; (b) The area of interest.

2.1.1. Data Source

The rainfall data utilized in this study is sourced from the Climate Hazards Group InfraRed Precipitation with Station (CHIRPS V2) dataset, available through the International Research Institute for Climate and Society (IRI) data portal. This quasi-global dataset offers daily temporal resolution and a spatial resolution of 0.25˚ × 0.25˚, covering the period from 1981 to 2023. Developed through collaboration between the US Geological Survey (USGS) and the Earth Resources Observation and Science (EROS) Center, CHIRPS integrates satellite imagery with high-resolution (0.05˚) and in situ station data, using an algorithm that blends

various temporal resolutions of cold cloud duration (CCD) precipitation. It is widely used for climate impact assessments, including flood and drought monitoring, as well as trend analysis (Funk et al., 2015).

To investigate the influence of large-scale atmospheric and oceanic circulation patterns on precipitation extremes, we employed indices for the Atlantic Multidecadal Oscillation (AMO), Pacific Decadal Oscillation (PDO), El Niño–Southern Oscillation (ENSO), and the Indian Ocean Dipole (IOD). Monthly index data were obtained from the National Oceanic and Atmospheric Administration (NOAA) Physical Sciences Laboratory (available at: https://psl.noaa.gov). However, the data was averaged to have seasonal means covering the period of 1981–2023 to match the rainfall indices along the season of interest. Sea Surface Temperature (SST) data used in the study are derived from NOAA's Extended Reconstructed Sea Surface Temperature dataset (ERSST V5). This dataset offers monthly temporal resolution and a spatial resolution of 2˚ × 2˚, utilizing recent contributions from the International Comprehensive Ocean-Atmosphere Dataset (ICOADS) (Huang et al., 2017). Additionally meteorological data, including geopotential height and wind fields, were sourced from the European Centre for Medium-Range Weather Forecasts (ECMWF) ERA5 reanalysis dataset. ERA5 provides a horizontal resolution of 0.25˚ × 0.25˚, making it suitable for analyzing atmospheric dynamics linked to precipitation variability.

2.1.2. Data Quality Control

To ensure the reliability and consistency of the rainfall data before calculating extreme precipitation indices and conducting trend analysis, rigorous data quality control and homogeneity assessments were performed. The RClimDex package (Zhang et al., 2004) and the RHtest package (Wang et al., 2007) were employed for these evaluations. Both tools are widely recognized and recommended by the World Meteorological Organization (WMO) for processing meteorological data and analyzing extreme climate indices (Tian et al., 2017). These methods effectively identify and correct potential inconsistencies, ensuring that the dataset is suitable for robust climate variability and trend analysis.

2.2. Methodology

2.2.1. Calculation of Indices

To detect and assess precipitation extremes, this study utilized nine precipitation extreme indices (**Table 1**) from a framework established by the Expert Team on Climate Change Detection and Indices (ETCCDI), details available on the website (http://etccdi.pacificclimate.org/indices.shtml), the Climate Variability and Predictability (CLIVAR) research program, and the Joint WMO-CCI Technical Commission for Oceanography and Marine Meteorology (JCOMM) (Karl et al., 1999). This framework includes 27 standardized extreme climate indices derived from daily temperature and precipitation data. These indices are widely endorsed and have been employed in numerous studies to analyze climate extremes e.g. (Li et al., 2018; Manzanas et al., 2014; Santos et al., 2012; Sheikh et al., 2015; Tian et al., 2017; van den Besselaar et al., 2013; Wang et al., 2017; Zhang et al., 2001).

Table 1. Definition of 9 extreme precipitation indices used for the study.

ID	Index name	Definition	Units
SDII	Daily precipitation intensity	Annual mean rainfall with (RR ≥ 1 mm)	mm/day
R10mm	Number of heavy precipitation days	Number of days when PRCP ≥ 10 mm/year	days
RX5day	Maximum 5-day precipitation	Maximum consecutive 5-day precipitation per year	mm
CDD	Consecutive dry days	Maximum number of consecutive days with RR < 1 mm	days
CWD	Consecutive wet days	Maximum number of consecutive days with RR > 1 mm	days
PRCPTOT	Annual total precipitation on wet days	Annual total rainfall on wet day (RR ≥ 1 mm)	mm
R95Ptot	Very wet day	Annual total PRCP when (RR ≥ 95p)	mm
R99pTOT	Extremely wet day	Annual total PRCP when RR ≥ 95p	mm
Rx1day	Daily maximum rainfall	Monthly maximum 1-day precipitation	mm

Additionally, this study incorporated key large-scale climate indices to investigate oceanic influences on precipitation extremes. The Atlantic Multidecadal Oscillation (AMO) index was calculated by averaging sea surface temperature (SST) anomalies in the North Atlantic (north of the equator). The Pacific Decadal Oscillation (PDO) index was derived from the leading principal component of monthly SST anomalies in the North Pacific Ocean (north of 20˚N). El Niño–Southern Oscillation (ENSO) was represented using the Niño 3.4 SST index, reflecting average SST anomalies in the east-central tropical Pacific (5˚S - 5˚N, 170˚W - 120˚W). The Indian Ocean Dipole (IOD) was tracked using the Dipole Mode Index (DMI), which measures the SST anomaly difference between the western (50˚ - 70˚E, 10˚S - 10˚N) and southeastern (90˚ - 110˚E, 10˚S - 0˚) equatorial Indian Ocean.

2.2.2. Trend Analysis

In climate and hydrology research, trend analysis serves as a fundamental approach for uncovering patterns within time-series data. The Mann–Kendall test, a well-established non-parametric method (Kendall, 1955; Mann, 1945), is commonly employed for this purpose. This test assumes that the data are independent, randomly ordered, and free from serial correlations. Endorsed by the World Meteorological Organization (WMO), the Mann–Kendall test is widely applied to identify significant monotonic trends in hydrometeorological time series, particularly in studies of extreme events (Ahmad et al., 2018; Li et al., 2018; Tian et al., 2017). To quantify the magnitude of detected trends, Sen's slope estimator is frequently utilized (Sen, 1968). Statistical significance is assessed by comparing calculated p-values against a predefined threshold of 0.05, corresponding to a 95% confidence level. Trends with p-values below this threshold are deemed significant, while those exceeding it are considered insignificant.

2.2.3. Correlation between Precipitation Extremes Indices and Large-Scale Patterns of Atmospheric and Ocean Circulation

To investigate the spatial and temporal patterns of precipitation extremes within

the study area, Empirical Orthogonal Function (EOF) analysis was employed. This method, also referred to as Principal Component Analysis (PCA), is widely used in climate research to examine the structural characteristics of matrix data. Specifically, EOF analysis was applied to assess the mean spatial and temporal variability of rainfall during the November-to-April period. The technique decomposes the dataset into orthogonal spatial patterns, known as EOFs, and their associated time series, referred to as Principal Components (PCs). The underlying premise of EOF analysis is that signals with greater variance are often the most significant.

The procedure involves calculating the eigenvalues and eigenvectors of the spatially weighted anomaly covariance matrix of the field. Previous studies have demonstrated the utility of EOF analysis in examining precipitation variability in East Africa, including Tanzania (Limbu & Guirong, 2020; Makula & Zhou, 2022). To explore potential relationships between precipitation indices and oceanic variables, Pearson correlation coefficients were computed between sea surface temperature (SST) anomalies over oceanic basins and the summed first two principal components of rainfall indices in the region. Additionally, correlations between extreme precipitation indices and key oceanic systems were analyzed to assess the influence of oceanic drivers on regional climate extremes.

3. Results and Discussion

3.1. Climatological Means for Precipitation Extremes

The spatial patterns of wet and dry spell indices across the study region reveal significant variability in rainfall characteristics and extreme events. **Figure 2(a)** shows the distribution of consecutive dry days (CDD), where most areas experience values below 60 days. This suggests relatively short dry periods across the region, with exceptions in the far southern parts where dry spells may extend to 60 - 80 days. These dry periods are an indication of regions less prone to prolonged drought. In contrast, **Figure 2(b)** depicting consecutive wet days (CWD) shows a marked difference. The southern and central regions exhibit prolonged wet spells, exceeding 110 days, which suggests persistent rainy conditions in these areas. Meanwhile, northern zones record shorter wet periods, generally ranging between 50 and 90 days, highlighting regional differences in rainfall persistence. **Figure 2(c)** reveals the distribution of total precipitation (PRCPTOT), with the central regions receiving substantial rainfall, often exceeding 1300 mm. In contrast, the northern regions receive significantly less precipitation, with totals generally ranging from 450 to 750 mm. This north-south gradient highlights the disparity in water availability across the region.

Figure 2(d) depicts the number of extreme rainfall days (R10mm), where the central areas towards south experience between 30 and 64 days of extreme rainfall. The northern regions, in contrast, see fewer than 24 extreme days. **Figure 2(e)** shows R95pTOT (rainfall from very wet days), with values exceeding 100 mm in the northern regions. Finally, **Figure 2(f)** illustrates the simple daily intensity

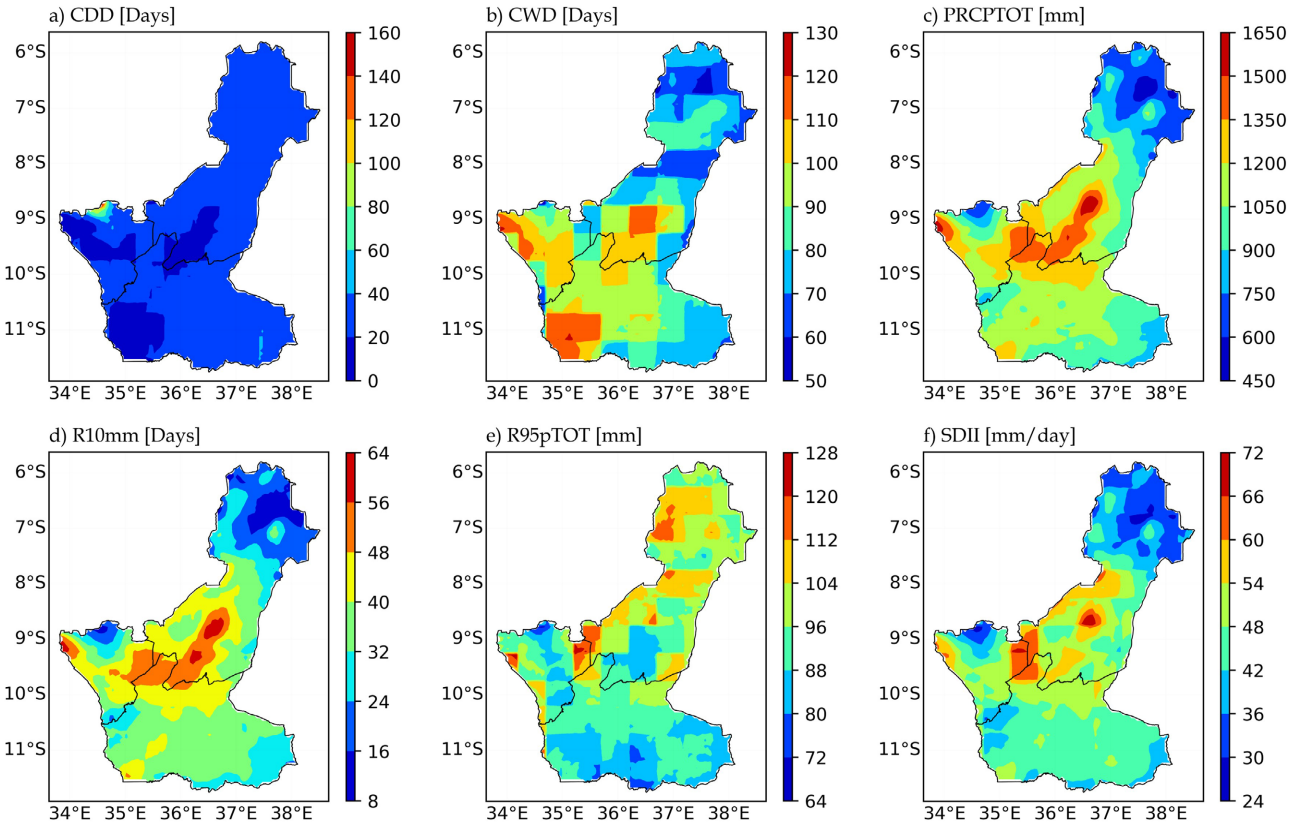

Figure 2. Spatial distributions of the climatological mean of precipitation Extreme Indices over the study region during 1981-2023.

index (SDII), where central areas show rainfall intensities surpassing 66 mm/day, indicating localized heavy rainfall events. These findings underscore the need for targeted water resource management and flood mitigation strategies in regions prone to both extreme rainfall and prolonged wet periods, especially in the southern and central zones.

3.2. Trends

The analysis of rainfall trends reveals pronounced spatial variability in wet and dry spells across the study region. Consecutive dry days (CDD); (**Figure 3(a)**) demonstrate a significant decreasing trend in the southern and western areas, suggesting shorter drought periods. In contrast, the northeastern and central regions show an insignificant increasing trend, indicating a potential lengthening of dry spells. Consecutive wet days (CWD); (**Figure 3(b)**) exhibit significant positive trends over most of the region, with only a few small, isolated areas showing no notable changes, implying an overall increase in the duration of wet periods.

Trends in total annual precipitation (PRCPTOT) (**Figure 3(c)**) indicate significant increases over the central and northern regions, reflecting higher rainfall levels. Meanwhile, southern areas display declining precipitation totals, highlighting emerging challenges related to water scarcity. Similarly, extreme rainfall days (R10mm); (**Figure 3(d)**) show a rising trend in the central and northern regions, elevating flood risks, whereas southern areas experience fewer such events,

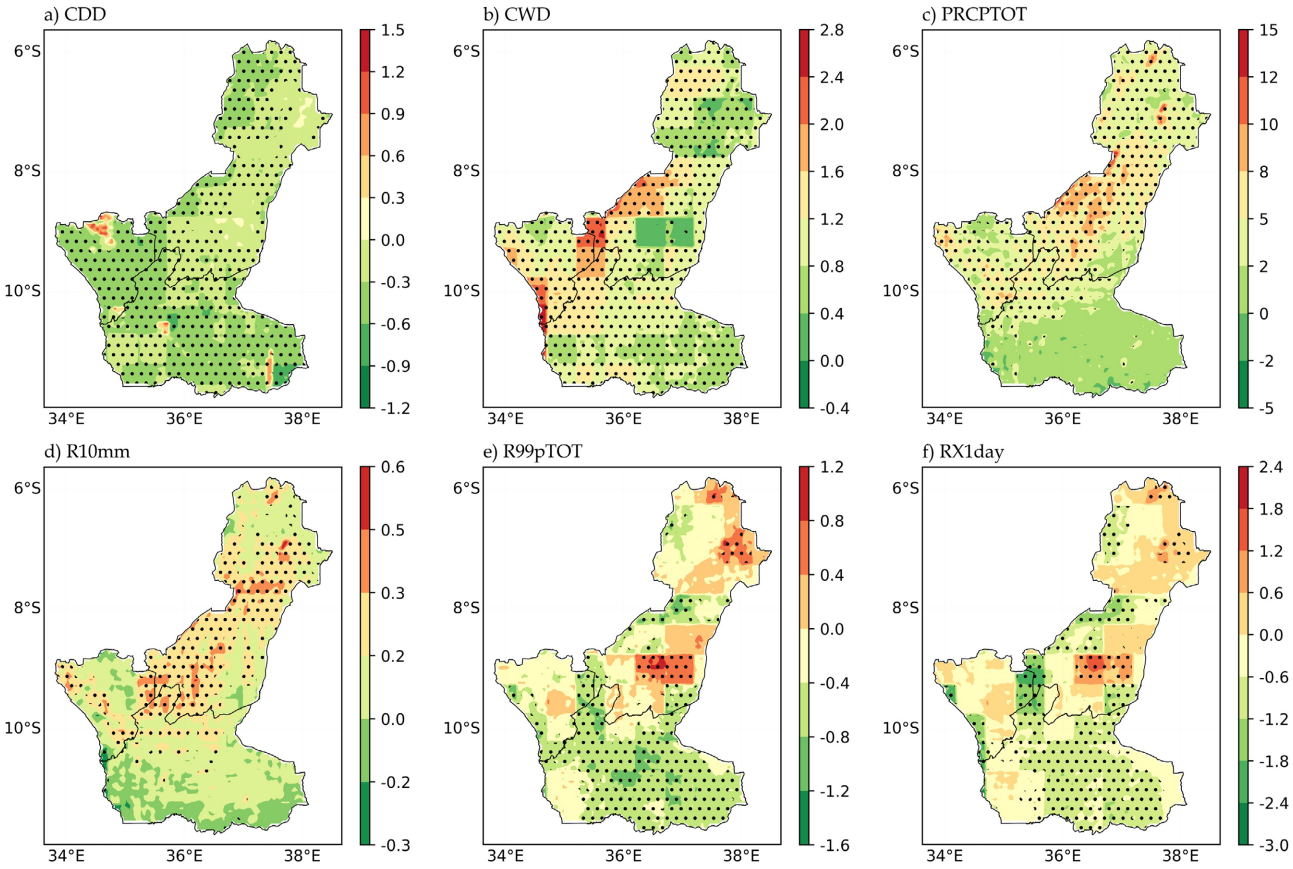

Figure 3. Spatial distributions of the linear trends of precipitation Extreme Indices over the study region during 1981-2023. Dotted areas are significant at the 0.05 significance level according to the student's t test.

reducing flood risk but exacerbating water shortages. Rainfall from very wet days (R99pTOT) and maximum one-day precipitation (RX1day); (**Figure 3(e)** and **Figure 3(f)**) follow comparable patterns, with significant declines in the southern region and insignificant to significant increases in the central and northern areas. These trends underscore the importance of tailored water management strategies. Addressing the growing disparities in rainfall patterns is essential to mitigate flood risks in wetter regions while ensuring sustainable water availability in drier areas.

3.3. Spatiotemporal Characteristics

Aiming at obtaining the typical spatial characteristics of extreme climate and its annual variation, the leading EOF modes and the corresponding time series are analyzed in this section. The analysis of the first empirical orthogonal function (EOF1) and its associated principal components (PCs) offers a comprehensive understanding of climate variability over time. By examining indices such as R95pTOT, CDD, CWD, PRCPTOT, R10mm, and RX5day, we can identify both spatial patterns and temporal trends. These trends are indicative of inter-annual and inter-decadal variations in climate, providing insights into long-term shifts in precipitation and extreme weather events across the study region.

The R95pTOT index accounts for 36% of total variance (**Figure 4(a)**) which

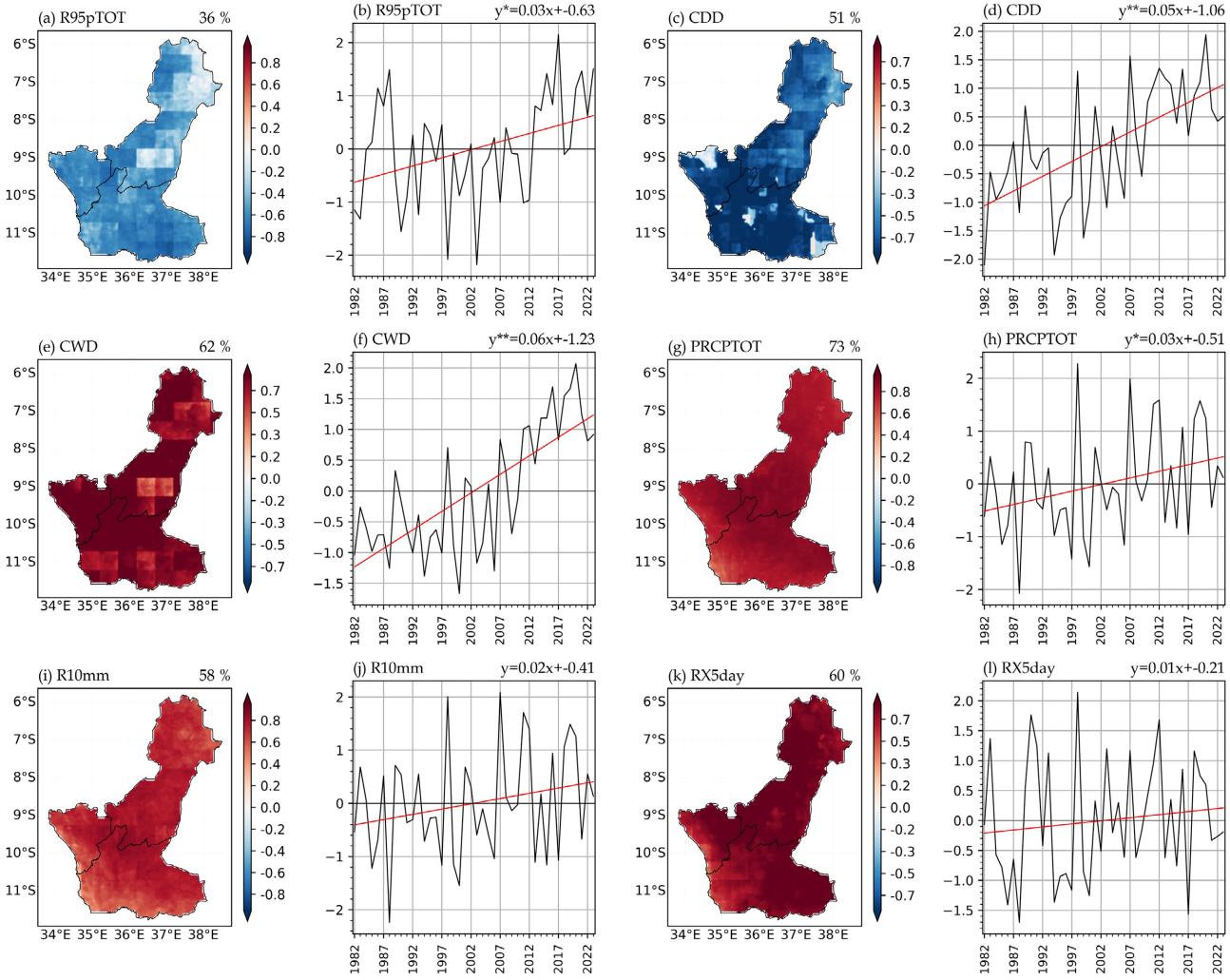

Figure 4. Spatial patterns of the first leading EOF (EOF1) mode and the time series of the first principal component (PC1) over the study region during 1981-2023. The marks of * and ** over the letter y represent that the linear regression equation is significant at 0.05 and 0.01 significance levels, respectively.

measures the proportion of precipitation from extreme events, shows predominantly negative anomalies across the region, with less variability over southern part suggesting a decrease in extreme precipitation events over the study period. The time series reveals a gradual inter-decadal increasing tendency according to the linear tendency analysis (**Figure 4(b)**), with a slight positive slope indicating that extreme precipitation events are becoming more frequent over the long term despite an overall decrease in the frequency of extreme wet days. This suggests a subtle shift toward more intense precipitation events in the later decades. The CDD index quantifies consecutive dry days, accounts for 51% of total variance (**Figure 4(c)**) and it exhibits significant inter-decadal variations, with a marked decrease in dry days over the study period. The southern region shows the strongest negative anomalies which is reflected in the linear trend in the time series (**Figure 4(d)**). This suggests long-term trends towards increased aridity in the southern parts of the region, with a gradual shift toward more persistent dry spells over

the decades. The inter-annual variability in CDD shows substantial fluctuations, with years of significantly dry conditions interspersed with wetter years. For CWD, which represents consecutive wet days, (**Figure 4(e)**) accounts for 62% of the total variance, a significant positive anomaly is evident in the northern and central regions, indicating a long-term trend toward increased wet spells. The spatial pattern shows darker red shades in these areas, which align with the positive trend in the time series (**Figure 4(f)**). This trend indicates an inter-decadal increase in the duration and frequency of consecutive wet days, particularly in the central and southern parts of the region. On an inter-annual scale, there are variabilities in wet spells, but the overall long-term trend points to increased wet conditions in these areas.

Similarly, the PRCPTOT index which reflects total annual precipitation, (**Figure 4(g)**) which accounts for 73% of total variance exhibits the increases in the central regions, with positive anomalies observed almost over the whole study region. This suggests that over the last few decades, these regions have experienced an overall increase in total precipitation. The time series (**Figure 4(h)**) shows a positive trend with a slope of 0.03, reinforcing the idea that these regions are becoming wetter over time. While the inter-annual variability is notable, particularly during extreme years with higher precipitation, the long-term trend reflects an increase in precipitation totals, particularly in the central and southern parts of the region. The R10mm index which measures the frequency of extreme rainfall events (greater than 10mm), accounts for 58% of total variance (**Figure 4(i)**) reveals an inter-decadal increase in extreme rainfall days, The spatial distribution shows positive anomalies in the areas, with the time series confirming a slight upward trend in extreme rainfall days (**Figure 4(j)**). This suggests that over the long term, these areas are experiencing more frequent and intense rainfall events. The inter-annual fluctuations are evident, with some years showing significantly higher numbers of extreme rainfall days, but the general trend points to an increase in extreme rainfall intensity in the regions. Finally, the RX5day index which quantifies rainfall events over 5-day periods, accounts for 60% of total variance (**Figure 4(k)**) shows a spatial pattern with significant positive anomalies across the study region, indicating increased intensity of 5-day rainfall events in the area. The time series demonstrates a gradual positive trend (slope of 0.01), suggesting that over the study period, the intensity of 5-day rainfall events has increased (**Figure 4(l)**). While there is noticeable inter-annual variation, with occasional years exhibiting extreme rainfall, the overall inter-decadal trend points to a shift towards more intense and frequent 5-day extreme rainfall events.

The second leading EOF reveals a prominent north-south dipole pattern in both spatial and temporal variability across the analyzed precipitation indices. For R95pTOT, the spatial map highlights significant reductions in extreme precipitation totals over the northern region, contrasted by increases in the south (**Figure 5(a)**), with the time series showing a statistically significant downward trend over the study period (**Figure 5(b)**). Conversely, consecutive dry days (CDD) exhibit

positive anomalies in the northern region and negative anomalies in the south (Figure 5(c)), reflecting a tendency toward longer dry spells in the north. The temporal evolution of CDD displays a weak upward trend (Figure 5(d)). with notable inter-annual variability. In contrast, continuous wet days (CWD) demonstrate a modest positive trend (Figure 5(f)) over time, particularly in the northern areas where the spatial anomalies are more pronounced (Figure 5(e)).

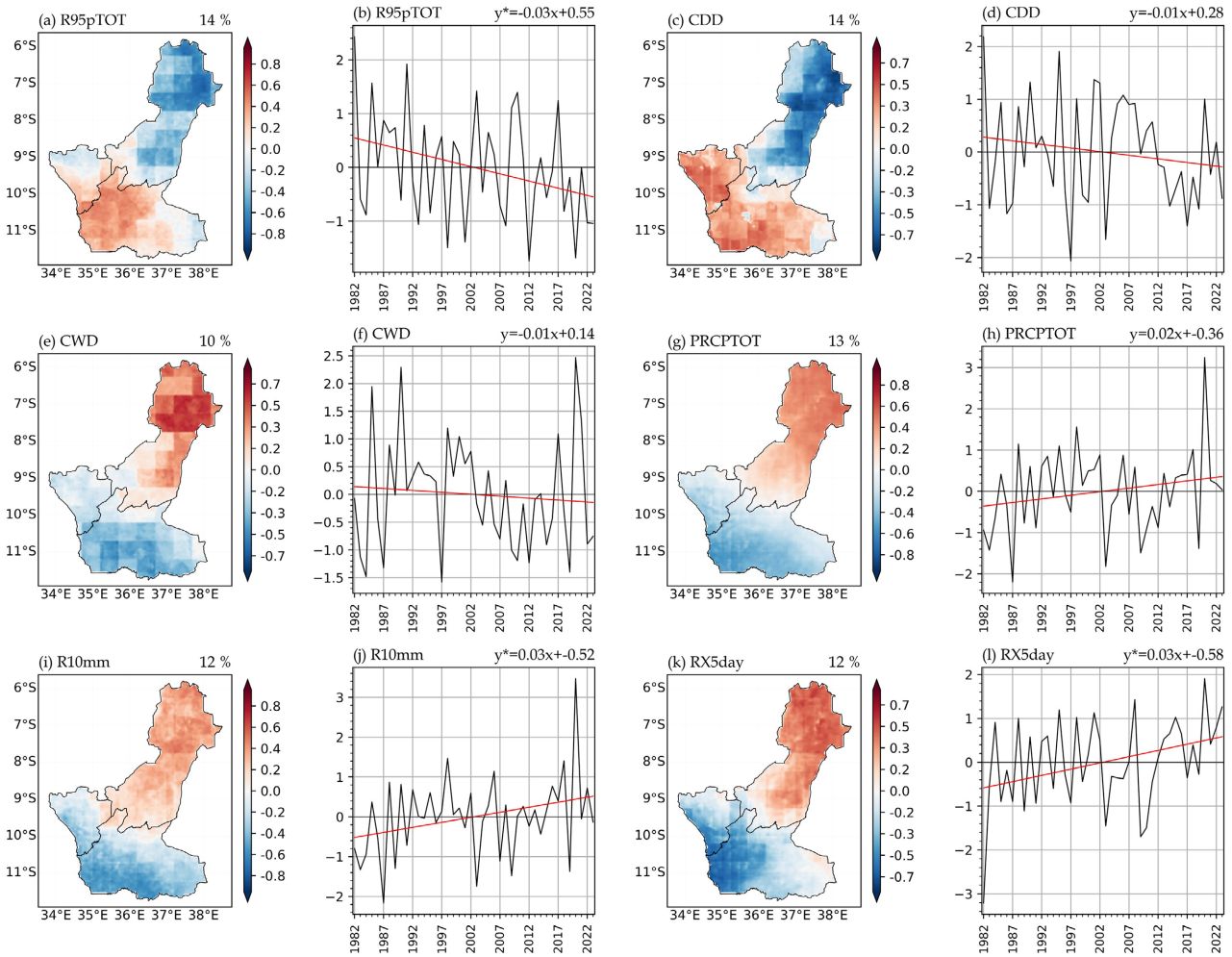

Figure 5. Spatial patterns of the second leading EOF (EOF2) mode and the time series of the second principal component (PC2) over the study region during 1981-2023. The marks of * over the letter y represent that the linear regression equation is significant at 0.05 significance levels.

The total precipitation (PRCPTOT) exhibits a northward increase and a southward decline, corroborating the spatial pattern (Figure 5(g)), with its time series indicating a gradual upward trend (Figure 5(h)). Similarly, heavy precipitation indices, including R10mm and RX5day, show significant increases in the northern region (Figure 5(i) and Figure 5(k)), supported by positive trends in their respective time series (Figure 5(j) and Figure 5(l)) respectively. These results suggest a notable rise in the frequency and magnitude of extreme precipitation events in the north, accompanied by a contrasting reduction in the south. Overall, the second

EOF underscores the interplay between wet and dry extremes, revealing strong inter-annual variability modulated by long-term inter-decadal trends. The findings point toward a changing climate regime characterized by increasing precipitation extremes in the north and a heightened propensity for dry conditions in the southern areas.

4. Possible Impacts from Oceanic Systems

Numerous studies have demonstrated that temperature and precipitation extremes are influenced by anomalous atmospheric circulation patterns, which are, in turn, modulated by large-scale oceanic systems such as the Atlantic Multidecadal Oscillation (AMO), Pacific Decadal Oscillation (PDO), El Niño-Southern Oscillation (ENSO), and Indian Ocean Dipole (IOD) (Gao et al., 2019; Lu et al., 2006; Shi et al., 2018; Yu et al., 2016) To evaluate the potential impacts of these oceanic systems on extreme events within the study area, this analysis calculates correlations between the principal components (PC1 and PC2) of precipitation extremes and the indices of these oceanic systems. The results of these correlations are presented in Table 2.

Table 2. Correlation coefficients of the PC1 and PC2 for the precipitation extreme indices and the oceanic systems indices during 1981-2023.

Extreme Indices	AMO	PDO	ENSO	IOD
PCI				
CDD	0.55**	0.22	0.33*	−0.24
CWD	0.64**	0.13	0.24	0.54**
R10mm	0.32	−0.18	0.57**	0.29
PC2				
R10mm	0.19	−0.27	0.35*	0.23
R95Ptot	0.35*	0.09	0.27	0.03
SDII	0.36*	0.32*	0.02	0.35*

Only indices with at least one correlation passing the significance test are presented; *Significant at the 0.05 significance level; **Significant at the 0.01 significance level.

The leading principal component (PC1) uncovers critical relationships illustrating how the Atlantic Multidecadal Oscillation (AMO) and El Niño-Southern Oscillation (ENSO) phases influence extreme dry and wet conditions. For instance, the Consecutive Dry Days (CDD) index exhibits a strong positive correlation with AMO (0.55, significant at the 0.01 level), indicating that warm AMO phases are associated with extended dry periods. This finding suggests that warm AMO phases may exacerbate drought conditions by contributing to prolonged dry spells. Similarly, CDD shows a moderate positive correlation with ENSO (0.33, significant at the 0.05 level), implying that El Niño events, known to alter regional precipitation patterns, may also lead to extended dry periods. These re-

sults highlight the roles of both AMO and ENSO in modulating dry spell variability, with AMO exerting a more pronounced influence. In contrast, the Consecutive Wet Days (CWD) index demonstrates strong positive correlations with both AMO (0.64) and the Indian Ocean Dipole (IOD) (0.54), both significant at the 0.01 level. This indicates that positive AMO phases foster sustained wet conditions, while positive IOD phases contribute to prolonged periods of consecutive wet days by enhancing regional moisture availability. The combined impact of these oscillations underscores their significance in prolonged wet conditions, with AMO playing a more dominant role. For the R10mm index, which represents days with rainfall exceeding 10 mm, ENSO emerges as a key driver in its PC1 mode. ENSO exhibits a strong positive correlation with R10mm (0.57, significant at the 0.01 level), suggesting that moderate rainfall events become more frequent during specific ENSO phases, particularly El Niño. This relationship highlights ENSO's capacity to intensify moderate rainfall events, likely through atmospheric circulation mechanisms that amplify precipitation.

The second leading principal component (PC2) highlights additional relationships, particularly the interactions of ENSO and AMO with various aspects of precipitation intensity. In the PC2 mode of R10mm, ENSO exhibits a moderate positive correlation (0.35, significant at the 0.05 level), indicating that ENSO's influence on moderate rainfall events extends into this secondary mode of precipitation variability. This suggests a nuanced role of ENSO in modulating rainfall patterns beyond its primary mode of variability. For R95pTOT, AMO also demonstrates a moderate positive correlation (0.35, significant at the 0.05 level). This relationship implies that positive AMO phases may enhance extreme precipitation totals, potentially contributing to greater rainfall during these events. The SDII in PC2 reveals significant correlations with both AMO (−0.36) and PDO (0.32), each at the 0.05 level. These findings suggest that positive AMO phases may suppress daily precipitation intensity, while positive PDO phases may amplify it. This dual influence underscores the contrasting roles of AMO and PDO in shaping daily precipitation dynamics, reflecting their opposing effects on rainfall intensity within the region.

To further investigate the connections between oceanic systems and precipitation extremes, the spatial distribution of correlation coefficients was analyzed between the principal components (PCs) of Empirical Orthogonal Function (EOF) modes and the sea surface temperatures (SSTs), as well as lower-level circulation patterns and geopotential height fields (**Figure 6** and **Figure 7**). Various studies have been conducted in different regions including Tanzania using these parameters (Fan et al., 2022; Mafuru & Guirong, 2018; Makula & Zhou, 2021; Massawe & Xiao, 2021). This analysis concentrated on PCs that exhibited statistically significant correlations at the 0.01 and 0.05 levels, as summarized in **Table 2**. The spatial correlation patterns reveal that global SST anomalies, particularly those associated with major climate modes such as ENSO, IOD, AMO, and PDO, play a critical role in driving extreme precipitation variability. SST anomalies in the

equatorial Pacific, strongly linked to ENSO phases, show pronounced correlations with several precipitation extremes. During El Niño phases, extreme precipitation intensifies in some regions and diminishes in others, consistent with observed variability in dry spell (CDD) (Figure 6(a)), and wet spell (CWD) (Figure 6(b)) patterns. Furthermore, ENSO's influence on indices such as R10mm (Figure 6(c)), underscores its pivotal role in modulating both the intensity and frequency of rainfall events across the study area. The Indian Ocean Dipole (IOD) also exhibits a significant influence, with positive SST anomalies in the Indian Ocean correlating with indices like CWD (Figure 6(b)), and R10mm (Figure 6(d)). This suggests that positive IOD phases enhance consecutive wet days and moderate precipitation events, likely by increasing regional moisture availability. The impacts of AMO and PDO, while more subtle than those of ENSO or IOD, are evident in correlations over the North Atlantic and northern Pacific.

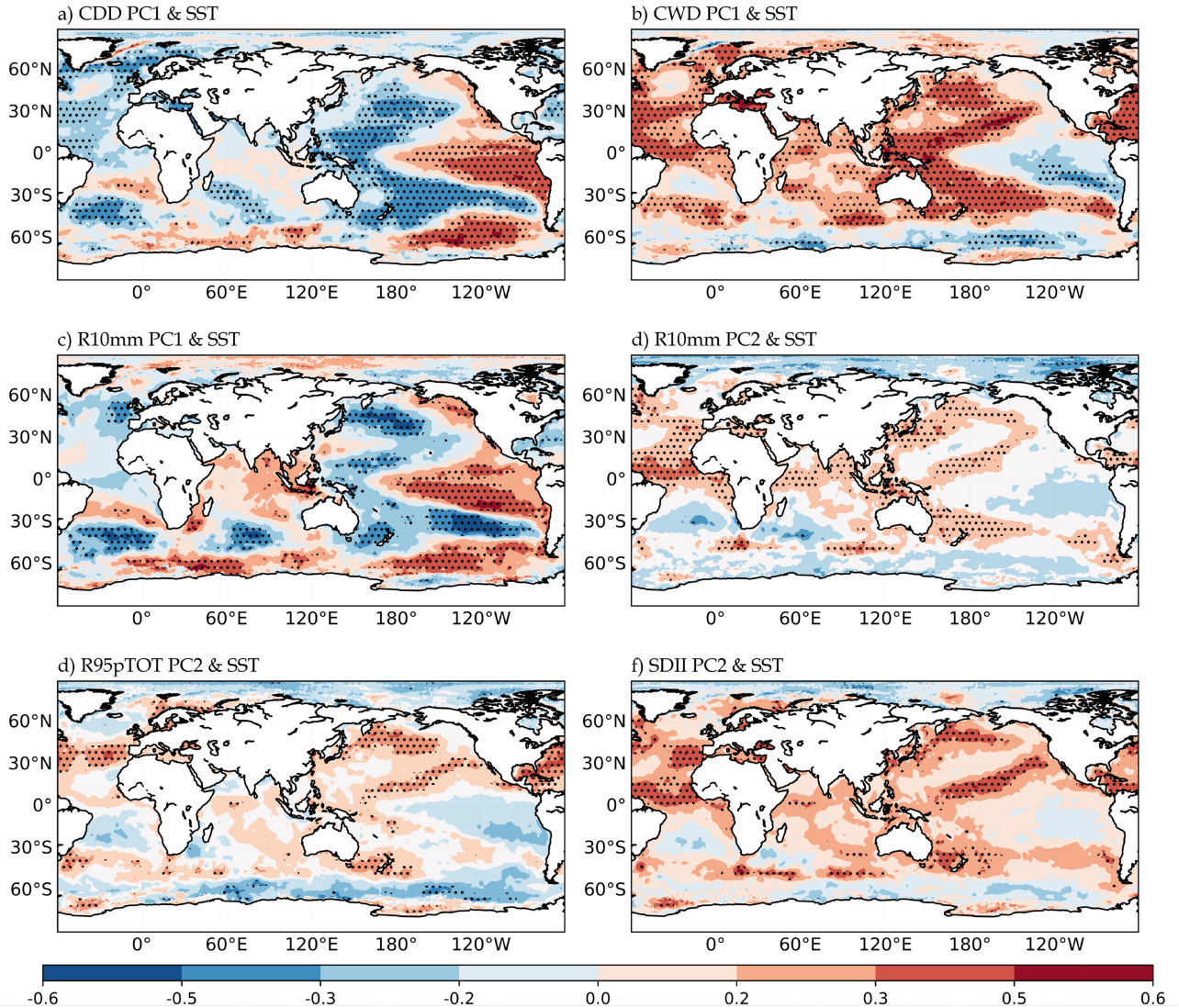

Figure 6. The correlation coefficient between SST and the PCs over the study region during 1981-2023. Dotted areas are significant at the 0.05 significance level according to the student's *t* test.

These patterns suggest that the decadal SST variability associated with AMO and PDO influences regional precipitation extremes, particularly CDD. These longer-term oscillations appear to shape the baseline climate state, upon which shorter-term modes like ENSO and IOD operate, thereby modulating extended periods of dryness or wetness.

The positive correlations between CDD PC1 and Z850 over the North Pacific and North Atlantic (**Figure 7(a)**) highlight the role of persistent high-pressure systems in these regions. High geopotential height anomalies, characteristic of anticyclonic subsidence, suppress convective activity, fostering stable and dry conditions. These pronounced positive correlations suggest that high-pressure ridges are dominant features during extended dry periods, limiting moisture convergence. Supporting this, wind vector patterns exhibit divergence away from high-pressure centers, reinforcing atmospheric stability and reducing the likelihood of

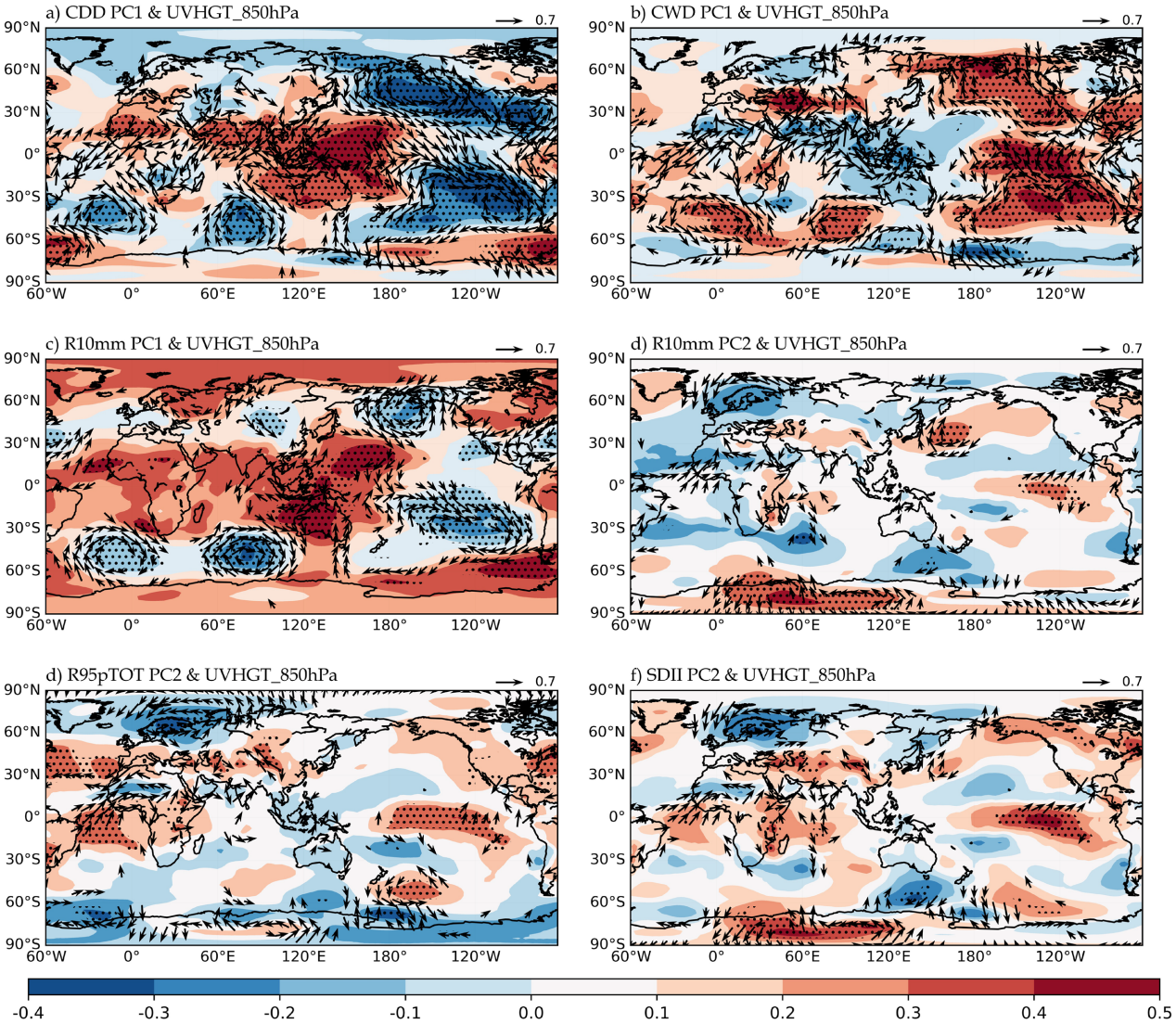

Figure 7. The correlation coefficients between 850 hPa geopotential height (shaded), 850 hPa wind (vector) and the PCs during 1981-2023. Dotted areas and plotted wind vectors are significant at the 0.05 significance level according to the student's *t* test.

rainfall. These findings underscore the strong linkage between CDD and large-scale anticyclonic circulations that inhibit precipitation.

In contrast, CWD PC1 (Figure 7(b)) shows significant positive correlations over the eastern Indian Ocean and western Pacific, indicative of low-level cyclonic circulation patterns favorable to prolonged wet periods. The associated positive height anomalies in the western Pacific, coupled with cyclonic flow, suggest enhanced moisture transport from surrounding oceanic regions, facilitating convergence and convective activity. This relationship highlights the role of cyclonic systems in sustaining consecutive wet days. For moderate precipitation events (R10mm PC1), positive Z850 height anomalies are observed over the North Atlantic and North Pacific (Figure 7(c)), along with a cyclonic circulation pattern in the equatorial Pacific. These patterns indicate that moderate rainfall events are linked to moisture advection from tropical to extratropical regions. The low-level cyclonic circulation over the equatorial Pacific may reflect the influence of the Walker Circulation and ENSO, particularly El Niño phases, which disrupt typical moisture distribution patterns, enhancing moderate rainfall in areas with reinforced warm SSTs and convection. R10mm PC2 exhibits a more localized influence, with positive Z850 anomalies over the western Pacific and central Atlantic (Figure 7(d)). While these regions display cyclonic flow patterns, they are less pronounced compared to PC1, suggesting that R10mm PC2 captures variability influenced by localized SST anomalies and transient atmospheric features rather than dominant global-scale signals. Extreme precipitation totals (R95pTOT PC2) correlate with positive Z850 anomalies in the North Atlantic and central Pacific (Figure 7(e)). This pattern suggests the involvement of extratropical storm tracks and tropical-subtropical teleconnections. High geopotential heights in these regions appear to act as steering mechanisms for mid-latitude cyclones and facilitate moisture transport. The observed correlations imply that extreme rainfall events are influenced by broad atmospheric circulation patterns, interacting with regional climate modes such as the North Atlantic Oscillation (NAO) and Pacific Decadal Oscillation (PDO). These modes affect the trajectory and intensity of storm systems that drive extreme precipitation. The SDII PC2 index, depicted in (Figure 7(f)), represents daily rainfall intensity and is associated with positive height anomalies over parts of the North Atlantic and Pacific, alongside cyclonic flow in the equatorial Pacific. This spatial pattern indicates that daily precipitation intensity in these regions is influenced by an interplay between tropical and extratropical systems. The cyclonic flow over the equatorial Pacific likely reflects the impact of ENSO, which enhances convective activity and moisture availability, thereby intensifying precipitation in this region. Conversely, the positive Z850 anomalies over the North Atlantic suggest atmospheric stability in the extratropic, which may influence the frequency and intensity of convective systems responsible for extreme rainfall events. This combination of tropical moisture transport and extratropical atmospheric modulation underscores the multi-scale drivers of daily precipitation variability captured by SDII PC2.

5. Conclusion

This study examined the climatological means, trends, and spatial-temporal variations of precipitation extremes over the study region during 1981 to 2023, alongside the potential influences of oceanic systems. The key findings are as follows:

1) The region exhibits notable spatial patterns and trends in extreme precipitation (Ndabagenga et al., 2023). Central and southern areas experience more intense and frequent rainfall, with higher values for consecutive wet days, heavy precipitation events, and maximum daily precipitation intensities. These areas also show upward trends in precipitation indices indicating an increase in both the frequency and intensity of extreme rainfall events over time. In contrast, the northern region experiences fewer wet spells and lower overall precipitation, suggesting a marked regional contrast, with central and southern areas being more vulnerable to extreme wet conditions.

2) Empirical Orthogonal Function (EOF) analysis reveals two principal components (PCs) that capture distinct modes of precipitation variability. EOF1 identifies a spatial pattern where southern regions exhibit higher variability in extreme precipitation events, while central areas experience more intense precipitation. This component highlights the concentration of intense precipitation in the southern and central regions. EOF2, however, indicates a north-south gradient, with the northern regions more influenced by moderate, sustained precipitation events, while the southern regions are characterized by intense, short-duration rainfall. These principal components encapsulate the complex spatial distribution and temporal variability of extreme precipitation across the region.

3) Climate oscillations, such as the Atlantic Multidecadal Oscillation (AMO), El Niño-Southern Oscillation (ENSO), Indian Ocean Dipole (IOD), and Pacific Decadal Oscillation (PDO), play a crucial role in shaping regional precipitation patterns. Positive phases of IOD are associated with increased wet conditions, similar results were obtained by (Borhara et al., 2020), while ENSO, particularly during El Niño events, drives an increase in moderate rainfall and alters the spatial distribution of precipitation extremes. The PDO affects daily precipitation intensity, with impacts that contrast with those of AMO. These climate drivers significantly influence the frequency and intensity of extreme precipitation, underlining the role of large-scale climatic phenomena in modulating regional precipitation dynamics.

4) Correlation analysis between precipitation indices and atmospheric circulation patterns reveals key interactions between large-scale pressure systems and precipitation variability. High-pressure systems in the North Pacific and North Atlantic, associated with positive Z850 anomalies, promote dry conditions by inducing anticyclonic subsidence and limiting moisture convergence. In contrast, cyclonic circulations in the eastern Indian Ocean and western Pacific, linked to negative height anomalies, enhance wet conditions by facilitating moisture convergence and convective activity similar results to (Kavishe & Limbu, 2020). These patterns, influenced by ENSO and other climate modes, interact with sea surface

temperatures (SST) and geopotential height fields to drive regional precipitation extremes, illustrating the complex relationships between atmospheric dynamics and precipitation variability. This intricate interplay highlights the importance of both local and global climate drivers in shaping precipitation patterns and underscores the need for ongoing monitoring and adaptive strategies to manage the increasing risks associated with extreme precipitation events.

Acknowledgements

The first author would like to express sincere appreciation to the Ministry of Commerce of China (MOFCOM) and the Tanzania Meteorological Authority, for providing the opportunity to conduct this study. Special thanks are also extended to Zhao Yu for her supervision and invaluable guidance throughout the research.

Conflicts of Interest

The authors declare no conflicts of interest regarding the publication of this paper.

References

Ahmad, I., Zhang, F., Tayyab, M., Anjum, M. N., Zaman, M., Liu, J. et al. (2018). Spatio-temporal Analysis of Precipitation Variability in Annual, Seasonal and Extreme Values over Upper Indus River Basin. *Atmospheric Research, 213,* 346-360. https://doi.org/10.1016/j.atmosres.2018.06.019

Alexander, L. V. (2016). Global Observed Long-Term Changes in Temperature and Precipitation Extremes: A Review of Progress and Limitations in IPCC Assessments and beyond. *Weather and Climate Extremes, 11,* 4-16. https://doi.org/10.1016/j.wace.2015.10.007

Alexander, L. V., Zhang, X., Peterson, T. C., Caesar, J., Gleason, B., Klein Tank, A. M. G. et al. (2006). Global Observed Changes in Daily Climate Extremes of Temperature and Precipitation. *Journal of Geophysical Research: Atmospheres, 111,* D05109. https://doi.org/10.1029/2005jd006290

Ame, H. K., Kijazi, A. L., Changa, L. B., Mafuru, K. B., Ngwali, M. K., Faki, M. M. et al. (2021). Rainfall Variability over Tanzania during October to December and Its Association with Sea Surface Temperature (SST). *Atmospheric and Climate Sciences, 11,* 324-341. https://doi.org/10.4236/acs.2021.112019

Barrett, C. B., & Santos, P. (2014). The Impact of Changing Rainfall Variability on Resource-Dependent Wealth Dynamics. *Ecological Economics, 105,* 48-54. https://doi.org/10.1016/j.ecolecon.2014.05.009

Borhara, K., Pokharel, B., Bean, B., Deng, L., & Wang, S. S. (2020). On Tanzania's Precipitation Climatology, Variability, and Future Projection. *Climate, 8,* Article No. 34. https://doi.org/10.3390/cli8020034

Brohan, P., Kennedy, J. J., Harris, I., Tett, S. F. B., & Jones, P. D. (2006). Uncertainty Estimates in Regional and Global Observed Temperature Changes: A New Data Set from 1850. *Journal of Geophysical Research: Atmospheres, 111,* D12106. https://doi.org/10.1029/2005jd006548

Chang'a, L. B., Kijazi, A. L., Luhunga, P. M., Ng'ongolo, H. K., & Mtongor, H. I. (2017). Spatial and Temporal Analysis of Rainfall and Temperature Extreme Indices in Tanzania. *Atmospheric and Climate Sciences, 7,* 525-539.

https://doi.org/10.4236/acs.2017.74038

Elleder, L. (2015). Historical Changes in Frequency of Extreme Floods in Prague. *Hydrology and Earth System Sciences, 19,* 4307-4315. https://doi.org/10.5194/hess-19-4307-2015

Fan, K., Xu, Z., & Tian, B. (2014). Has the Intensity of the Interannual Variability in Summer Rainfall over South China Remarkably Increased? *Meteorology and Atmospheric Physics, 124,* 23-32. https://doi.org/10.1007/s00703-013-0301-5

Fan, Y., Li, J., Zhu, S., Li, H., & Zhou, B. (2022). Trends and Variabilities of Precipitation and Temperature Extremes over Southeast Asia during 1981-2017. *Meteorology and Atmospheric Physics, 134,* Article No. 78. https://doi.org/10.1007/s00703-022-00913-6

Fischer, E. M., & Knutti, R. (2015). Anthropogenic Contribution to Global Occurrence of Heavy-Precipitation and High-Temperature Extremes. *Nature Climate Change, 5,* 560-564. https://doi.org/10.1038/nclimate2617

Funk, C., Peterson, P., Landsfeld, M., Pedreros, D., Verdin, J., Shukla, S. et al. (2015). The Climate Hazards Infrared Precipitation with Stations—A New Environmental Record for Monitoring Extremes. *Scientific Data, 2,* Article ID: 150066. https://doi.org/10.1038/sdata.2015.66

Gao, M., Yang, J., Gong, D., Shi, P., Han, Z., & Kim, S. (2019). Footprints of Atlantic Multidecadal Oscillation in the Low-Frequency Variation of Extreme High Temperature in the Northern Hemisphere. *Journal of Climate, 32,* 791-802. https://doi.org/10.1175/jcli-d-18-0446.1

Gautam, R. C., & Bana, R. S. (2014). Drought in India: Its Impact and Mitigation Strategies—A Review. *Indian Journal of Agronomy, 59,* 179-190. https://www.IndianJournals.com

Huang, B., Thorne, P. W., Banzon, V. F., Boyer, T., Chepurin, G., Lawrimore, J. H. et al. (2017). Extended Reconstructed Sea Surface Temperature, Version 5 (ersstv5): Upgrades, Validations, and Intercomparisons. *Journal of Climate, 30,* 8179-8205. https://doi.org/10.1175/jcli-d-16-0836.1

Karl, T. R., Nicholls, N., & Ghazi, A. (1999). Fitting a Probability Distribution to Extreme Precipitation for a Limited Mountain Area in Vietnam. *Climatic Change, 42,* 3-7. https://doi.org/10.1023/a:1005491526870

Kavishe, G. M., & Limbu, P. T. S. (2020). Variation of October to December Rainfall in Tanzania and Its Association with Sea Surface Temperature. *Arabian Journal of Geosciences, 13,* Article No. 534. https://doi.org/10.1007/s12517-020-05535-z

Kendall, M. G. (1955). Further Contributions to the Theory of Paired Comparisons. *Biometrics, 11,* 43-62. https://doi.org/10.2307/3001479

Kijazi, A. L., & Reason, C. J. C. (2009). Analysis of the 2006 Floods over Northern Tanzania. *International Journal of Climatology, 29,* 955-970. https://doi.org/10.1002/joc.1846

Lavell, A., Oppenheimer, M., Diop, C., Hess, J., Lempert, R., Li, J., Muir-Wood, R., & Myeong, S. (2012). Climate Change: New Dimensions in Disaster Risk, Exposure, Vulnerability, and Resilience. In C. B. Field, V. Barros, T. F. Stocker, D. Qin, D.J. Dokken, K. L. Ebi, M. D. Mastrandrea, K. J. Mach, G.-K. Plattner, S. K. Allen, M. Tignor, & P. M. Midgley (Eds.), *Managing the Risks of Extreme Events and Disasters to Advance Climate Change Adaptation* (pp. 25-64). Cambridge University Press.

Li, G., Zhang, X., Cannon, A. J., Murdock, T., Sobie, S., Zwiers, F. et al. (2018). Indices of Canada's Future Climate for General and Agricultural Adaptation Applications. *Climatic Change, 148,* 249-263. https://doi.org/10.1007/s10584-018-2199-x

Li, X., Wang, X., & Babovic, V. (2018). Analysis of Variability and Trends of Precipitation

Extremes in Singapore during 1980-2013. *International Journal of Climatology, 38,* 125-141. https://doi.org/10.1002/joc.5165

Limbu, P. T. S., & Guirong, T. (2020). Influence of the Tropical Atlantic Ocean and Its Walker Circulation Cell on October-December Rainfall Variability over Tanzania. *International Journal of Climatology, 40,* 5767-5782. https://doi.org/10.1002/joc.6550

Lu, R., Dong, B., & Ding, H. (2006). Impact of the Atlantic Multidecadal Oscillation on the Asian Summer Monsoon. *Geophysical Research Letters, 33,* L24701. https://doi.org/10.1029/2006gl027655

Mafuru, K. B., & Guirong, T. (2018). Assessing Prone Areas to Heavy Rainfall and the Impaction of the Upper Warm Temperature Anomaly during March-May Rainfall Season in Tanzania. *Advances in Meteorology, 2018,* Article ID: 8353296. https://doi.org/10.1155/2018/8353296

Makula, E. K., & Zhou, B. (2021). Changes in March to May Rainfall over Tanzania during 1978-2017. *International Journal of Climatology, 41,* 5663-5675. https://doi.org/10.1002/joc.7146

Makula, E. K., & Zhou, B. (2022). Linkage of Tanzania Short Rain Variability to Sea Surface Temperature over the Southern Oceans. *Frontiers in Earth Science, 10,* Article ID: 922172. https://doi.org/10.3389/feart.2022.922172

Mallakpour, I., & Villarini, G. (2015). The Changing Nature of Flooding across the Central United States. *Nature Climate Change, 5,* 250-254. https://doi.org/10.1038/nclimate2516

Mann, H. B. (1945). Nonparametric Tests against Trend. *Econometrica, 13,* 245-259. https://doi.org/10.2307/1907187

Manzanas, R., Amekudzi, L. K., Preko, K., Herrera, S., & Gutiérrez, J. M. (2014). Precipitation Variability and Trends in Ghana: An Intercomparison of Observational and Reanalysis Products. *Climatic Change, 124,* 805-819. https://doi.org/10.1007/s10584-014-1100-9

Massawe, W. C., & Xiao, Z. (2021). Analysis of Rainfall Variability over Tanzania in Late Austral Summer. *Atmospheric and Oceanic Science Letters, 14,* Article ID: 100049. https://doi.org/10.1016/j.aosl.2021.100049

Nangombe, S., Zhou, T., Zhang, W., Wu, B., Hu, S., Zou, L. et al. (2018). Record-Breaking Climate Extremes in Africa under Stabilized 1.5 ˚C and 2 ˚C Global Warming Scenarios. *Nature Climate Change, 8,* 375-380. https://doi.org/10.1038/s41558-018-0145-6

Ndabagenga, D. M., Yu, J., Mbawala, J. R., Ntigwaza, C. Y., & Juma, A. S. (2023). Climatic Indices' Analysis on Extreme Precipitation for Tanzania Synoptic Stations. *Journal of Geoscience and Environment Protection, 11,* 182-208. https://doi.org/10.4236/gep.2023.1112010

Nicholson, S. E. (2015). Long-Term Variability of the East African "Short Rains" and Its Links to Large-Scale Factors. *International Journal of Climatology, 35,* 3979-3990. https://doi.org/10.1002/joc.4259

Nicholson, S. E. (2018). The ITCZ and the Seasonal Cycle over Equatorial Africa. *Bulletin of the American Meteorological Society, 99,* 337-348. https://doi.org/10.1175/bams-d-16-0287.1

O'Gorman, P. A. (2015). Precipitation Extremes under Climate Change. *Current Climate Change Reports, 1,* 49-59. https://doi.org/10.1007/s40641-015-0009-3

Otto, F. E. L. (2024). *Annual Review of Environment and Resources Attribution of Weather and Climate Events.*

Rosenzweig, C., Tubiello, F. N., Goldberg, R., Mills, E., & Bloomfield, J. (2002). Increased Crop Damage in the US from Excess Precipitation under Climate Change. *Global Envi-*

ronmental Change, 12, 197-202. https://doi.org/10.1016/s0959-3780(02)00008-0

Santos, C. A. C. d., Brito, J. I. B. d., Júnior, C. H. F. d. S., & Dantas, L. G. (2012). Trends in Precipitation Extremes over the Northern Part of Brazil from ERA40 Dataset. *Revista Brasileira de Geografia Física, 5,* 836-851. https://doi.org/10.26848/rbgf.v5i4.232872

Sen, P. K. (1968). Estimates of the Regression Coefficient Based on Kendall's Tau. *Journal of the American Statistical Association, 63,* 1379-1389. https://doi.org/10.1080/01621459.1968.10480934

Sharma, S., Hamal, K., Khadka, N., Ali, M., Subedi, M., Hussain, G. et al. (2021). Projected Drought Conditions over Southern Slope of the Central Himalaya Using CMIP6 Models. *Earth Systems and Environment, 5,* 849-859. https://doi.org/10.1007/s41748-021-00254-1

Sheikh, M. M., Manzoor, N., Ashraf, J., Adnan, M., Collins, D., Hameed, S. et al. (2015). Trends in Extreme Daily Rainfall and Temperature Indices over South Asia. *International Journal of Climatology, 35,* 1625-1637. https://doi.org/10.1002/joc.4081

Shi, J., Cui, L., Wen, K., Tian, Z., Wei, P., & Zhang, B. (2018). Trends in the Consecutive Days of Temperature and Precipitation Extremes in China during 1961-2015. *Environmental Research, 161,* 381-391. https://doi.org/10.1016/j.envres.2017.11.037

Shiu, C., Liu, S. C., Fu, C., Dai, A., & Sun, Y. (2012). How Much Do Precipitation Extremes Change in a Warming Climate? *Geophysical Research Letters, 39,* L17707. https://doi.org/10.1029/2012gl052762

Tian, J., Liu, J., Wang, J., Li, C., Nie, H., & Yu, F. (2017). Trend Analysis of Temperature and Precipitation Extremes in Major Grain Producing Area of China. *International Journal of Climatology, 37,* 672-687. https://doi.org/10.1002/joc.4732

Trenberth, K. (2011). Changes in Precipitation with Climate Change. *Climate Research, 47,* 123-138. https://doi.org/10.3354/cr00953

van den Besselaar, E. J. M., Klein Tank, A. M. G., & Buishand, T. A. (2013). Trends in European Precipitation Extremes over 1951-2010. *International Journal of Climatology, 33,* 2682-2689. https://doi.org/10.1002/joc.3619

Wang, X. L., Wen, Q. H., & Wu, Y. (2007). Penalized Maximal T Test for Detecting Undocumented Mean Change in Climate Data Series. *Journal of Applied Meteorology and Climatology, 46,* 916-931. https://doi.org/10.1175/jam2504.1

Wang, X., Hou, X., & Wang, Y. (2017). Spatiotemporal Variations and Regional Differences of Extreme Precipitation Events in the Coastal Area of China from 1961 to 2014. *Atmospheric Research, 197,* 94-104. https://doi.org/10.1016/j.atmosres.2017.06.022

Yu, L., Zhong, S., Pei, L., Bian, X., & Heilman, W. E. (2016). Contribution of Large-Scale Circulation Anomalies to Changes in Extreme Precipitation Frequency in the United States. *Environmental Research Letters, 11,* Article ID: 044003. https://doi.org/10.1088/1748-9326/11/4/044003

Zhang, X. B., Yang, F., Alexander, L., Zwiers, F., Gleason, B., Stephenson, D., Klan Tank, A., New, M., & Vincent, L. (2004). *RClimDex (1.0) User Manual.*

Zhang, X., Hogg, W. D., & Mekis, É. (2001). Spatial and Temporal Characteristics of Heavy Precipitation Events over Canada. *Journal of Climate, 14,* 1923-1936. https://doi.org/10.1175/1520-0442(2001)014<1923:satcoh>2.0.co;2